Transfer of active motion from medium to probe via the induced friction and noise

Ji-Hui Pei (裴继辉) [1,2] and Christian Maes [1,*]

[1] *Department of Physics and Astronomy, KU Leuven, 3000, Belgium*
[2] *School of Physics, Peking University, Beijing, 100871, China*

Can activity be transmitted from smaller to larger scales? We report on such a transfer from a homogeneous active medium to a Newtonian spherical probe. The active medium consists of faster and dilute self-propelled particles, modeled as run-and-tumble particles in 1D or as active Brownian particles in 2D. We derive the reduced fluctuating dynamics of the probe, valid for arbitrary probe velocity, characterized by velocity-dependent friction and noise. In addition to a standard passive regime, we identify peculiar active regimes where the probe becomes self-propelled with high persistence, and its velocity distribution begets peaks at nonzero values. These features are quantitatively confirmed by numerical simulations of the composite probe-medium system. The emergence of active regimes depends not only on the far-from-equilibrium nature of the medium but also on the probe-medium coupling. Our findings reveal how, solely via the induced friction and noise, persistence can cross different scales to transfer active motion.

Introduction. Bridging different levels of physical description is a hallmark of statistical mechanics. Understanding how properties of microscopic evolutions, when combined with statistical considerations, penetrate the realm of mesoscopic and macroscopic physics and give rise to new emerging phenomena is one of the biggest challenges. A specific and important paradigm is the Brownian motion of a micron-sized colloidal particle suspended in a fluid at rest, where the environment is passive and the fluctuating motion is purely thermal. In this work, we explore a similar setup but with an active environment, uncovering very different reduced dynamics.

Active systems [1–7] drive themselves far from equilibrium by local energy consuming processes [5]. To investigate how active systems influence phenomena at a larger scale of length, mass or time, studying a heavy probe immersed in an active medium (or active bath) has attracted a lot of attention [7–55].

A scalar active medium can be modeled as a collection of self-propelled particles that show persistence in velocity, such as run-and-tumble and active Brownian particles [56–62]. While we know how an equilibrium bath leads to a passive probe motion, we enquire here whether and how a probe can inherit active motion from an active bath, that is, endowed with a persistent velocity. To fully understand this question requires knowledge of the reduced dynamics for the probe after theoretically integrating out the active bath.

The problem of integrating out the motion of active particles can proceed via several methods [47, 52, 55, 63]. For an active bath consisting of effectively independent active particles, existing results [53–55, 64, 65] suggest the following (or similar) underdamped Brownian dynamics for a heavy spherical probe with mass M and velocity $\mathbf{v}$,

$$M\dot{\mathbf{v}} = -\gamma\mathbf{v} + \sqrt{2B}\,\boldsymbol{\xi}, \tag{1}$$

with linear friction coefficient γ, standard white noise $\boldsymbol{\xi}$ and its intensity B. Such dynamics with linear friction are valid only for small probe speeds. For an active medium, γ and B do not satisfy the standard Einstein relation [66, 67], and it has recently been found that the linear friction coefficient γ can be negative [7, 54, 65, 68], indicating that the probe would accelerate when starting from a small velocity. After acceleration to higher speed, friction can no longer be described in linear form $-\gamma\mathbf{v}$. Therefore, when $\gamma < 0$, the Brownian dynamics (1) fails. Obtaining the correct reduced fluctuating motion of a spherical probe in a scalar active medium has remained a significant unsolved problem.

In this Letter, we identify the cause of the breakdown of (1) and derive the corrected reduced dynamics through a frame transformation prior to a quasistatic expansion. This procedure yields three components: a first-order nonlinear velocity-dependent friction (also reported in [68]), its second-order correction, and a velocity-dependent noise. From the corrected reduced dynamics, we observe both a passive regime and the emergence of notable active regimes. In the active regimes, activity is transferred to the probe: a 1D probe follows run-and-tumble motion or run-and-stop motion, while a 2D probe either exhibits active Brownian motion or switches randomly between active and passive Brownian motions. These results for the reduced dynamics are quantitatively confirmed by simulations.

This activity transmission hinges on the probe-medium coupling and the dimension. Unlike 1D where a soft coupling is necessary, we find that realistic hardcore (Lennard-Jones) interactions suffice to transfer activity in 2D, and we provide an experimental proposal.

Setup and general structure. The active medium is spatially homogeneous and considered in a dilute limit, consisting of N independent overdamped self-propelled particles with positions $\mathbf{z}^a$ ($a = 1, \ldots, N$ labels different particles). We take a periodic boundary on $(-L/2, L/2]^d$. The infinite size corresponds to the limit of $L, N \to \infty$

with fixed low density $n = N/L^d$. The Newtonian underdamped probe has position $\mathbf{q}$ and velocity $\mathbf{v}$. The interaction force between medium particles and probe derives from an isotropic potential, $F(|\mathbf{q}-\mathbf{z}|) = -U'(|\mathbf{q}-\mathbf{z}|)$. The equations of motion are,

$$\begin{aligned} \mu\dot{\mathbf{z}}^a &= F(r^a)\hat{\mathbf{r}}^a + \mathbf{A}^a, \\ M\dot{\mathbf{v}} &= -\sum_{a=1}^{N} F(r^a)\hat{\mathbf{r}}^a, \quad \dot{\mathbf{q}} = \mathbf{v} \end{aligned} \tag{2}$$

where $\mathbf{A}^a$ represents independent (for now unspecified) self-propulsion forces on the individual active particles; $\mathbf{r}^a = \mathbf{z}^a - \mathbf{q}$ is the relative position between the a-th medium particle and the probe, and $\hat{\mathbf{r}}^a = \mathbf{r}^a/r^a$ denotes its direction. μ is the inverse mobility of medium particles. The probe mass M is assumed large. We aim at a reduced description for the probe.

Existing studies [53, 55, 64, 65] obtain the Brownian dynamics (1) by assuming a time-scale separation between the probe and the medium particles. Yet, that assumption is not always valid because position $\mathbf{q}$ may not change slowly; that is, $\mathbf{v} = \dot{\mathbf{q}}$ may not be small (although the velocity $\mathbf{v}$ itself is usually slow since $\dot{\mathbf{v}}$ is small for a heavy probe).

We address this problem by the following physical procedure. For a homogeneous medium, $\mathbf{q}$ can be eliminated by the change of variables $\mathbf{z}^a \to \mathbf{r}^a = \mathbf{z}^a - \mathbf{q}$, which shifts the medium motion to the moving reference frame where the probe remains at the origin. The equations of motion (2) now become

$$\begin{aligned} \mu\dot{\mathbf{r}}^a &= -\mu\mathbf{v} + F(r^a)\hat{\mathbf{r}}^a + \mathbf{A}^a, \\ M\dot{\mathbf{v}} &= -\sum_{a=1}^{N} F(r^a)\hat{\mathbf{r}}^a. \end{aligned} \tag{3}$$

The probe position $\mathbf{q}$ does not appear anymore. For a heavy probe, unlike position $\mathbf{q}$, the velocity $\mathbf{v}$ is always slow, and the time scale of $\mathbf{v}$ (τ_v) is much larger than that of the $\mathbf{r}^a$ (τ_r), characterized by a small constant $\epsilon = \tau_r/\tau_v$; see supplemental material (SM) [69].

We can thus start from (3) to safely integrate out the medium particles as in the usual quasistatic approximation. As explained in SM [69], up to $O(\epsilon^2)$, we obtain a nonlinear fluctuating dynamics [70] of the probe, where velocity-dependent friction and noise appear, all expressed as explicit correlation functions. This powerful reduced dynamics indicates that the active motion can be transmitted from the medium solely via the effects of friction and noise. It makes the theoretical treatment of modeling active particles by velocity-dependent friction and noise come true [57, 71]. In what follows, we focus on the reduced dynamics in 1D and 2D for specific active media.

1D run-and-tumble medium. In 1D, we consider an active medium consisting of run-and-tumble particles [58, 59, 61, 72]. The equation of motion (3) of one medium particle in the moving frame becomes

$$\mu\dot{r} = F(r) + \mu u\sigma - \mu v \tag{4}$$

where $\sigma = \pm 1$ flips randomly at a Poisson rate α, and it indicates the direction of the constant self-propulsion speed $u > 0$. After integrating out medium particles, the reduced dynamics of the probe is given by a nonlinear equation [69],

$$\begin{aligned} M\dot{v}(t) = &- f(v(t)) + \sqrt{2B(v(t))}\,\xi(t) \\ &- \frac{1}{M}G(v(t)) + \frac{1-\eta}{M}B'(v(t)), \end{aligned} \tag{5}$$

where $\xi(t)$ is a standard white noise; η depends on the discretization convention of the stochastic differential equation: $\eta = 0$ for Itô, $\eta = 1/2$ for Stratonovich, and $\eta = 1$ for anti-Itô. The last term originates from the multiplicative noise. The (first-order) nonlinear friction $f(v)$, the noise intensity $B(v)$, and the second-order correction of the friction $G(v)$ are given explicitly in the End Matter. They are all expressed as expectation values in the "fixed-v" dynamics (Eq. (4) with fixed v) of a single medium particle. The term $f(v)$ is of order ϵ, and its linear part $\gamma = f'(v)\big|_{v=0}$ recovers the friction coefficient in previous studies [69]. In that sense, we call f the nonlinear friction. On the other hand, $G(v)$ and $B(v)$ are of order ϵ^2. The total nonlinear friction up to $O(\epsilon^2)$ is then $g(v) = f(v) + G(v)/M$, where $G(v)/M$ can be ignored in a qualitative approach but not in a quantitative analysis. The presence of velocity-dependent friction and noise is the main characteristic of the above dynamics, making it valid for arbitrary v.

The positivity of the nonlinear friction $f(v)$ is not ensured, which may cause the active motion of the probe. In the End Matter, we provide an intuitive analysis of $f(v)$. There are two requirements for $f(v)$ to exhibit negative values: the persistence length of medium particles should be large compared to the interaction range, $u/\alpha \gg R$; the coupling should not be hardcore, so that medium particles can pass through the probe.

From expressions of f, B, and G, one can straightforwardly calculate them numerically [69]. For the calculation, we choose the probe-medium coupling to be a soft repulsive interaction $F(r) = k\sin(\pi r/R)$ for $|r| < R$ and $F(r) = 0$ for $|r| > R$, with range R and strength k. The plots of $f(v)$ and $B(v)$ are shown in Figs. 1(a)-(b). The singular turn over in Fig. 1(b) is explained in the End Matter. In SM [69], we supplement more figures, which help to show how the negative region in $f(v)$ depends on the medium persistence and the interaction strength.

The dynamics of the probe can be classified into different regimes according to the behavior of friction $f(v)$ (or more precisely $f(v) + G(v)/M$); see Figs. 1(a)-(b):
(R1) A standard passive regime: $f(v) > 0$ for any $v > 0$.
(R2a) A peculiar active regime: $f(v) < 0$ for small

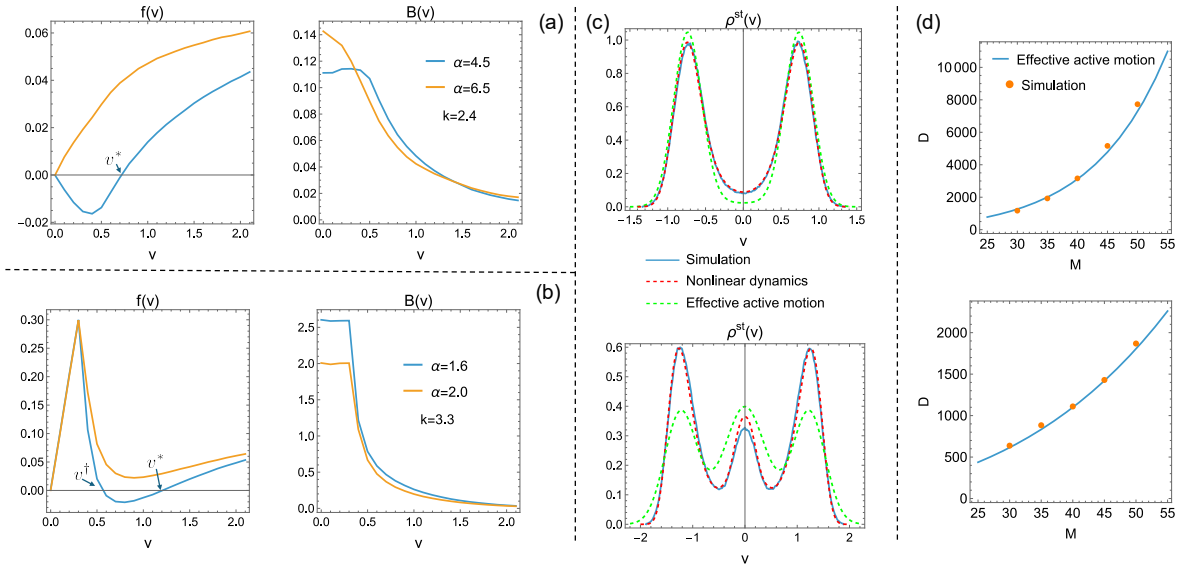


FIG. 1. For 1D run-and-tumble medium with interaction $F(r) = k\sin(\pi r/R)$ within range $r < R$: (a) Friction $f(v)$ and noise intensity $B(v)$ (per medium particle) with different flip rates α, showing regimes (R1) and (R2a). Parameters are $L = 10$, $R = 0.5$, $k = 2.4$, $u = 3$, $\mu = 1$. (b) Same for $k = 3.3$, corresponding to regimes (R1) and (R2b). (c) Stationary velocity distribution $\rho^{\rm st}(v)$ of the probe, from the simulation (blue), from the nonlinear dynamics (5) (red dashed), and from the effective active dynamics (green dashed). The upper panel corresponds to the blue line ($k = 2.4$, $\alpha = 4.5$) in (a) with probe mass $M = 30$, and the lower panel corresponds to the blue line ($k = 3.3$, $\alpha = 1.6$) in (b) with probe mass $M = 40$. (d) Diffusion coefficient of the probe for different mass: from the effective active motion (blue line) and the simulation (orange points). The upper panel and lower panel share the same parameters with the blue lines in (a) and (b), respectively.

$0 < v < v^*$ and $f(v) > 0$ for large $v > v^*$.

(R2b) Another peculiar active regime: $f(v) > 0$ for $0 < v < v^\dagger$, $f(v) < 0$ for $v^\dagger < v < v^*$, and $f(v) > 0$ for $v > v^*$.

In the standard (passive) regime (R1), the probe velocity fluctuates around 0. Expanding $f(v) \sim f'(0)v = \gamma v$ and $B(v) \sim B(0)$, the dynamics can be described by (1), which is an underdamped passive Brownian motion.

In regime (R2a), the stationary velocity distribution is bimodal with peaks around $\pm v^*$, as shown in Fig. 1(c). Most of the time, the probe moves at velocity around $\pm v^*$. Occasionally, at random times, the velocity transits between $\pm v^*$. The transition rate α^* can be obtained from the exact mean first-passage time for (5),

$$\alpha^{*-1} = \int_{-v^*}^{v^*} \mathrm{d}y \int_{-\infty}^{y} \mathrm{d}z \frac{\exp[\psi(y) - \psi(z)]}{B(z)}, \qquad (6)$$

with effective potential $\psi(v) = \int^v \mathrm{d}w \left[\frac{Mf(w)+G(w)}{B(w)}\right]$; see SM [69]. We may approximate the above formula by the Kramers formula [73] if the transitions are rare. Furthermore, the probe motion (5) in regime (R2a) can be reduced to an underdamped run-and-tumble motion: expanding around v^* and taking into account the transition, we obtain

$$M\dot{v} = -\mu^*(v - \sigma^* v^*) + \sqrt{2B^*}\,\xi, \quad \sigma^* = \pm 1, \qquad (7)$$

where $\mu^* = f'(v^*)$ is the effective friction coefficient, $\sigma^* v^*$ represents the propulsion velocity of the probe, flipping randomly at rate α^*, and $\sqrt{2B^*}\xi = \sqrt{2B(v^*)}\xi$ is the translational noise. From (7), we analytically deduce the diffusion coefficient D of the probe,

$$D = \lim_{t\to\infty} \langle q(t)^2 \rangle / (2t) = v^{*2}/(2\alpha^*) + B^*/\mu^{*2}. \qquad (8)$$

According to (6), α^* decreases exponentially with the probe mass M, and hence, the diffusion is exponentially enhanced for large M.

Finally, in regime (R2b), there are three peaks in the stationary velocity distribution: $0, \pm v^*$. Two transition rates α_0^* (for $\pm v^* \to 0$) and α_1^* (for $0 \to \pm v^*$) can also be solved analytically [69]. The dynamics in (R2b) can be further reduced to an underdamped "run-and-stop motion", characterized by

$$M\dot{v} = -\mu^*_{\sigma^*}(v - \sigma^* v^*) + \sqrt{2B^*_{\sigma^*}}\,\xi, \quad \sigma^* = 0, \pm 1. \qquad (9)$$

$\mu^*_{\sigma^*} = f'(\sigma^* v^*)$ and $B^*_{\sigma^*} = B(\sigma^* v^*)$ now depend on the current value of σ^*. From this effective active dynamics, the diffusion coefficient is given by

$$D = \frac{2\alpha_1^*}{\alpha_0^* + 2\alpha_1^*}\left(\frac{v^{*2}}{\alpha_0^*} + \frac{B_1^*}{\mu_1^{*2}}\right) + \frac{\alpha_0^*}{\alpha_0^* + 2\alpha_1^*}\frac{B_0^*}{\mu_0^2}. \qquad (10)$$

So far, there are two levels of reduced descriptions, the reduced nonlinear dynamics (5) and the effective active dynamics (7)(9). The reduced nonlinear dynamics (5)

is completely quantitative and universally valid for all regimes. Compared with direct simulations for the composite probe-medium system, we find excellent agreement for both the stationary distributions of the probe velocity $\rho^{\rm st}(v)$ and the transition rate, respectively shown in Fig. 1(c) and in SM [69]. The effective active dynamics (7)(9) serve as semi-quantitative approximations in the respective peculiar regimes. In velocity space, its prediction of the stationary distribution $\rho^{\rm st}(v)$ deviates somewhat from the simulations, as shown in Fig. 1(c). In position space, it quantitatively predicts the diffusion coefficient, in excellent agreement with simulations; see Fig. 1(d). This description is useful for an intuitive understanding of the active behavior of the probe motion in regimes (R2a)(R2b).

2D active Brownian medium. We continue with active Brownian particles [60] for the medium. Supposing the probe velocity is (v_x, v_y), the dynamics (3) for one active Brownian particle in the moving frame is then

$$\begin{aligned} \mu\dot{r}_x &= F(r)\hat{r}_x + \mu u\cos\phi - \mu v_x, \\ \mu\dot{r}_y &= F(r)\hat{r}_y + \mu u\sin\phi - \mu v_y, \\ \dot{\phi} &= \sqrt{2\alpha}\xi, \end{aligned} \tag{11}$$

with propulsion speed u, and $\alpha > 0$ characterizing the persistence of the propulsion angle ϕ.

Adopting polar coordinates in velocity space (v, θ) for the probe, with $v_x = v\cos\theta, v_y = v\sin\theta$, we obtain the reduced nonlinear dynamics [69], given by

$$\begin{aligned} M\dot{v}(t) &= -f(v(t)) + \sqrt{2B_\parallel(v(t))}\xi_\parallel(t) \\ &\quad - \frac{1}{M}G(v(t)) + \frac{1-\eta}{M}B'_\parallel(v(t)) + \frac{B_\perp(v(t))}{Mv(t)}, \\ Mv(t)\dot{\theta}(t) &= \sqrt{2B_\perp(v(t))}\xi_\perp(t), \end{aligned} \tag{12}$$

where $\xi_\parallel$ and $\xi_\perp$ are independent standard white noises, respectively causing the fluctuation along and perpendicular to the current velocity. η depends on the discretization convention, same as in 1D. The last term in the first equation, $B_\perp/(Mv)$, originates from the use of polar velocity coordinates. The nonlinear friction $f(v)$, its second-order correction $G(v)$, and the velocity-dependent noise intensities $B_\perp(v), B_\parallel(v)$ are given explicitly as expectation values of a "fixed-$\mathbf{v}$" dynamics; see the End Matter. Except for $f(v)$ of order $O(\epsilon)$, the other terms are of order $O(\epsilon^2)$.

The nonlinear friction $f(v)$ may take negative values. However, the mechanism in 2D is much complicated than that in 1D since the medium particles can bypass the probe. In the End Matter, we include an intuitive explanation. For $f(v)$ to exhibit negative values, first, as in 1D, the persistence length should be large compared to the interaction length. Secondly (and different from 1D), the interaction can have a hardcore, but in this case, the force should decay slowly at large distances, instead of being a direct collision.

As an example, we investigate the Lennard-Jones potential, a realistic interaction with a hardcore. We numerically calculate all quantities and plot $f(v)$, $B_\parallel(v)$, and $B_\perp(v)$ in Figs. 2(a)-(b). The Lennard-Jones force is $F(r) = k/k_0[(R/r)^{13} - (R/r)^7]$ with R denoting the size of the probe and k representing the strength of the interaction [74]. k_0 is chosen to render $\min_r F(r) = -k$.

Similarly to 1D, there are three distinct regimes determined by the sign of $f(v)$:
(A1) A standard passive regime: $f(v) > 0$ for all $v > 0$.
(A2a) A peculiar active regime: $f(v) < 0$ for $v \in (0, v^*)$ and $f(v) > 0$ for $v > v^*$.
(A2b) Another active regime: $f(v) > 0$ for $v \in (0, v^\dagger)$, $f(v) < 0$ for $v \in (v^\dagger, v^*)$, and $f(v) > 0$ for $v > v^*$.
In the active regimes, the probe dynamics is distinct from 1D, which we specify next.

In the standard (passive) regime (A1), the probe is well described as an underdamped Brownian motion (1) with linear friction coefficient $\gamma = f'(0)$ and constant noise intensity $B = B_\parallel(0) = B_\perp(0)$.

In the active regime (A2a), the probe moves at a speed around v^*; see Fig. 2(c). Note the significant difference between 1D and 2D. The direction angle θ of the velocity changes continuously and follows a free diffusion. The dynamics can be further simplified to an active motion. Expanding $f(v)$ and $B(v)$ around v^*, we find the probe follows an effective active motion, described by

$$\begin{aligned} M\dot{v} &= -\mu^*(v - v^*) + \frac{B^*_\perp}{Mv} + \sqrt{2B^*_\parallel}\xi_\parallel, \\ Mv^*\dot{\theta} &= \sqrt{2B^*_\perp}\xi_\perp. \end{aligned} \tag{13}$$

This is a special kind of underdamped active Brownian motion, in which the propulsion direction aligns with the direction of the velocity, sharing a common rotational diffusion process. $\mu^* = f'(v^*)$ plays the role of friction coefficient, v^* represents the propulsion speed, and $B^*_\perp = B_\perp(v^*)$, $B^*_\parallel = B_\parallel(v^*)$ are noise intensities. From (13), the diffusion coefficient is obtained as

$$D = M^2 v^{*4}/(2B^*_\perp) + (B^*_\perp + B^*_\parallel)/(2\mu^{*2}). \tag{14}$$

Different from 1D, the diffusion is enhanced quadratically as M increase, instead of exponentially.

In the active regime (A2b), ignoring the noise, there are two stable speeds, 0 and v^*. The probe velocity stays around either $v = 0$ or $v = v^*$, with random transitions between them; see Fig. 2(c). Thus, the probe motion randomly switches between active and passive Brownian motions, described by (1) and (13), respectively. Two switching rates can also be obtained.

Again, the nonlinear dynamics (12) is completely quantitative, while the effective active motion (13) is semi-quantitative (qualitative for velocity distribution but quantitative for diffusion coefficient). See Fig. 2(c) and Fig. 2(d) for the comparison of velocity distribution and of diffusion coefficient, respectively.

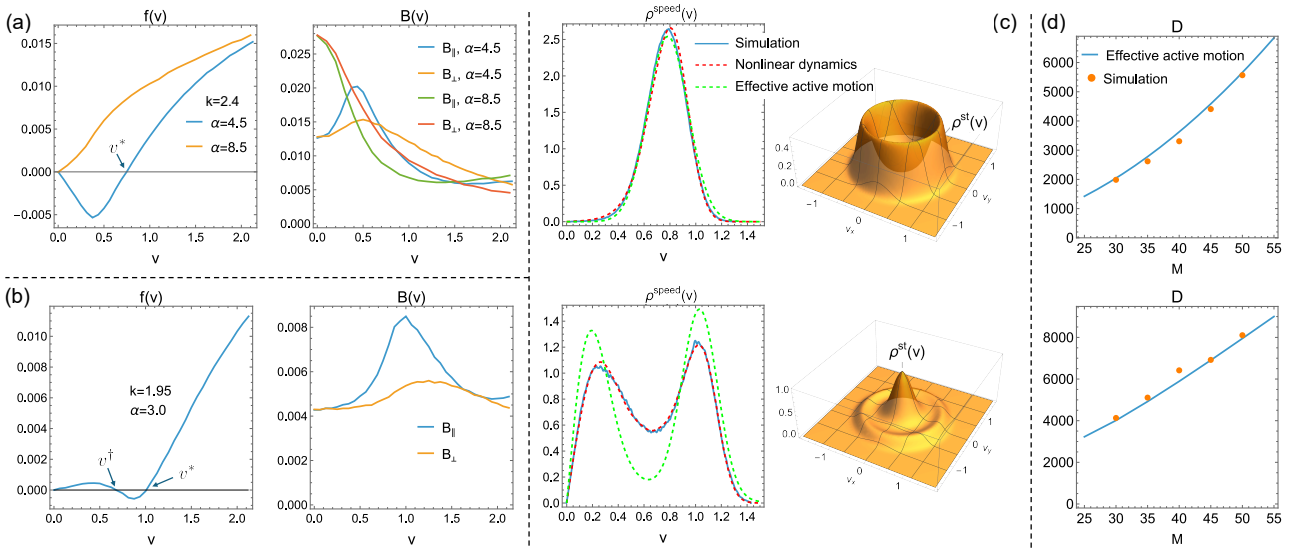


FIG. 2. For 2D active Brownian medium with Lennard-Jones interaction: (a) Landscapes of $f(v)$, $B_\parallel(v)$, and $B_\perp(v)$ (per medium particle) for different α, showing regimes (A1) and (A2a). Other parameters are $k = 2.4$, $u = 3$, $R = 0.5$, $L = 10$, $\mu = 1$. (b) Same for $k = 1.95$, $\alpha = 3.0$, corresponding to regime (A2b). (c) Stationary distributions of the probe velocity $\rho^{\rm st}(v_x, v_y)$ and speed $\rho^{\rm speed}(v) = 2\pi v \rho^{\rm st}(v_x, v_y)$. The 3D plots of $\rho^{\rm st}(v_x, v_y)$ and the red-dashed lines in $\rho^{\rm speed}(v)$ are obtained from the reduced dynamics (12). The blue line denotes the simulation results of the composite system. The green-dashed line is from the effective active motion. The upper panel corresponds to $k = 2.4$, $\alpha = 4.5$ in (a) and $M = 30$; the lower corresponds to $k = 1.95$, $\alpha = 3.0$ in (b) and $M = 46$. (d) Diffusion coefficient of the probe as a function of mass: from the effective active motion (blue line) and the simulation (orange points). The upper panel and lower panel correspond to $k = 2.4$, $\alpha = 4.5$ in (a) and $k = 1.95$, $\alpha = 3.0$ in (b), respectively.

Experimental proposal. Our theory requires an underdamped probe. The proper experimental systems can be active granular particles (for example, vibrobots in Ref. [26]) but not bacterial baths. Moreover, in 2D, a hardcore interaction should decay slowly at large distance to transfer activity, instead of being collisions. One scenario is to put a passive probe in a medium of active granular particles and to decorate the probe with silicon gel to soften the contact force. Meanwhile, we can use a magnetic probe and ferrous medium particles to realize a long-range attractive force. The two active regimes (A2a) and (A2b) can be achieved by tuning the relative magnitude between interaction and propulsion force of medium particles. By observing the velocity distribution, we can test whether the transfer of activity scenario works.

Conclusion. We present a complete solution to characterizing the reduced dynamics for a spherical probe immersed in a scalar active medium and find that active motion may be transmitted through the induced friction and noise for certain types of coupling. A related phenomenon was recently reported in a granular matter experiment [26].

Our study may prove constructive for designing artificial micro-devices working in an active (for instance, biological) environment. On a more fundamental level, the results are opening a new avenue for understanding the universal presence of active motion at different scales in nature. To conclude, these findings constitute important evidence for understanding the origin and transfer of active motion, where activity is begotten, not made.

Acknowledgments: This work received support from the China Scholarship Council, No. 202306010398.

* christian.maes@kuleuven.be

[1] J. Toner, Y. Tu, and S. Ramaswamy, Hydrodynamics and phases of flocks, Annals of Physics **318**, 170 (2005).
[2] S. Ramaswamy, The mechanics and statistics of active matter, Annual Review of Condensed Matter Physics **1**, 323 (2010).
[3] M. C. Marchetti, J. F. Joanny, S. Ramaswamy, T. B. Liverpool, J. Prost, M. Rao, and R. A. Simha, Hydrodynamics of soft active matter, Reviews of Modern Physics **85**, 1143 (2013).
[4] C. Bechinger, R. Di Leonardo, H. Löwen, C. Reichhardt, G. Volpe, and G. Volpe, Active particles in complex and crowded environments, Reviews of Modern Physics **88**, 045006 (2016).
[5] G. Gompper, R. G. Winkler, T. Speck, A. Solon, C. Nardini, F. Peruani, H. Löwen, R. Golestanian, U. B. Kaupp, L. Alvarez, T. Kirboe, E. Lauga, W. C. K. Poon, A. DeSimone, S. Muiños Landin, A. Fischer, N. A. Söker, F. Cichos, R. Kapral, P. Gaspard, M. Ripoll, F. Sagues, A. Doostmohammadi, J. M. Yeomans, I. S. Aranson, C. Bechinger, H. Stark, C. K. Hemelrijk, F. J. Nedelec, T. Sarkar, T. Aryaksama, M. Lacroix, G. Duclos, V. Yashunsky, P. Silberzan, M. Arroyo, and S. Kale, The

2020 motile active matter roadmap, Journal of Physics: Condensed Matter **32**, 193001 (2020).
[6] M. te Vrugt and R. Wittkowski, Metareview: a survey of active matter reviews, The European Physical Journal E **48**, 10.1140/epje/s10189-024-00466-z (2025).
[7] O. Granek, Y. Kafri, M. Kardar, S. Ro, J. Tailleur, and A. Solon, Colloquium : Inclusions, boundaries, and disorder in scalar active matter, Reviews of Modern Physics **96**, 031003 (2024).
[8] X.-L. Wu and A. Libchaber, Particle diffusion in a quasi-two-dimensional bacterial bath, Physical Review Letters **84**, 3017 (2000).
[9] D. T. N. Chen, A. W. C. Lau, L. A. Hough, M. F. Islam, M. Goulian, T. C. Lubensky, and A. G. Yodh, Fluctuations and rheology in active bacterial suspensions, Physical Review Letters **99**, 148302 (2007).
[10] K. C. Leptos, J. S. Guasto, J. P. Gollub, A. I. Pesci, and R. E. Goldstein, Dynamics of enhanced tracer diffusion in suspensions of swimming eukaryotic microorganisms, Physical Review Letters **103**, 198103 (2009).
[11] S. Rafaï, L. Jibuti, and P. Peyla, Effective viscosity of microswimmer suspensions, Physical Review Letters **104**, 098102 (2010).
[12] H. Kurtuldu, J. S. Guasto, K. A. Johnson, and J. P. Gollub, Enhancement of biomixing by swimming algal cells in two-dimensional films, Proceedings of the National Academy of Sciences **108**, 10391 (2011).
[13] C. Valeriani, M. Li, J. Novosel, J. Arlt, and D. Marenduzzo, Colloids in a bacterial bath: simulations and experiments, Soft Matter **7**, 5228 (2011).
[14] G. Miño, T. E. Mallouk, T. Darnige, M. Hoyos, J. Dauchet, J. Dunstan, R. Soto, Y. Wang, A. Rousselet, and E. Clément, Enhanced diffusion due to active swimmers at a solid surface, Physical Review Letters **106**, 048102 (2011).
[15] G. L. Miño, J. Dunstan, A. Rousselet, E. Clément, and R. Soto, Induced diffusion of tracers in a bacterial suspension: theory and experiments, Journal of Fluid Mechanics **729**, 423 (2013).
[16] A. Kaiser, A. Peshkov, A. Sokolov, B. ten Hagen, H. Löwen, and I. S. Aranson, Transport powered by bacterial turbulence, Physical Review Letters **112**, 158101 (2014).
[17] C. Maggi, M. Paoluzzi, N. Pellicciotta, A. Lepore, L. Angelani, and R. Di Leonardo, Generalized energy equipartition in harmonic oscillators driven by active baths, Physical Review Letters **113**, 238303 (2014).
[18] A. E. Patteson, A. Gopinath, P. K. Purohit, and P. E. Arratia, Particle diffusion in active fluids is non-monotonic in size, Soft Matter **12**, 2365 (2016).
[19] A. Argun, A.-R. Moradi, E. Pinçe, G. B. Bagci, A. Imparato, and G. Volpe, Non-Boltzmann stationary distributions and nonequilibrium relations in active baths, Physical Review E **94**, 062150 (2016).
[20] T. Kurihara, M. Aridome, H. Ayade, I. Zaid, and D. Mizuno, Non-Gaussian limit fluctuations in active swimmer suspensions, Physical Review E **95**, 030601 (2017).
[21] C. Maggi, M. Paoluzzi, L. Angelani, and R. Di Leonardo, Memory-less response and violation of the fluctuation-dissipation theorem in colloids suspended in an active bath, Scientific Reports **7**, 10.1038/s41598-017-17900-2 (2017).
[22] M. J. Y. Jerez, M. N. P. Confesor, M. V. Carpio Bernido, and C. C. Bernido, Anomalous diffusion of a probe in a bath of active granular chains, in *AIP Conference Proceedings*, Vol. 1871 (Author(s), 2017) p. 050004.
[23] J. Katuri, W. E. Uspal, M. N. Popescu, and S. Sánchez, Inferring non-equilibrium interactions from tracer response near confined active Janus particles, Science Advances **7**, 10.1126/sciadv.abd0719 (2021).
[24] S. Paul, A. Jayaram, N. Narinder, T. Speck, and C. Bechinger, Force generation in confined active fluids: The role of microstructure, Physical Review Letters **129**, 058001 (2022).
[25] D. Boriskovsky, B. Lindner, and Y. Roichman, The fluctuationdissipation relation holds for a macroscopic tracer in an active bath, Soft Matter **20**, 8017 (2024).
[26] L. Caprini, A. Ldov, R. K. Gupta, H. Ellenberg, R. Wittmann, H. Löwen, and C. Scholz, Emergent memory from tapping collisions in active granular matter, Communications Physics **7**, 10.1038/s42005-024-01540-w (2024).
[27] G. Grégoire, H. Chaté, and Y. Tu, Active and passive particles:modeling beads in a bacterial bath, Physical Review E **64**, 011902 (2001).
[28] D. Loi, S. Mossa, and L. F. Cugliandolo, Effective temperature of active matter, Physical Review E **77**, 051111 (2008).
[29] P. T. Underhill, J. P. Hernandez-Ortiz, and M. D. Graham, Diffusion and spatial correlations in suspensions of swimming particles, Physical Review Letters **100**, 248101 (2008).
[30] L. Angelani and R. D. Leonardo, Geometrically biased random walks in bacteria-driven micro-shuttles, New Journal of Physics **12**, 113017 (2010).
[31] G. Foffano, J. S. Lintuvuori, K. Stratford, M. E. Cates, and D. Marenduzzo, Colloids in active fluids: Anomalous microrheology and negative drag, Physical Review Letters **109**, 028103 (2012).
[32] S. A. Mallory, C. Valeriani, and A. Cacciuto, Curvature-induced activation of a passive tracer in an active bath, Physical Review E **90**, 032309 (2014).
[33] A. Suma, L. F. Cugliandolo, and G. Gonnella, Tracer motion in an active dumbbell fluid, Journal of Statistical Mechanics: Theory and Experiment **2016**, 054029 (2016).
[34] M. Kneevi and H. Stark, Effective Langevin equations for a polar tracer in an active bath, New Journal of Physics **22**, 113025 (2020).
[35] S. Ye, P. Liu, F. Ye, K. Chen, and M. Yang, Active noise experienced by a passive particle trapped in an active bath, Soft Matter **16**, 4655 (2020).
[36] J. Shea, G. Jung, and F. Schmid, Passive probe particle in an active bath: can we tell it is out of equilibrium?, Soft Matter **18**, 6965 (2022).
[37] Y. B. Dor, Y. Kafri, M. Kardar, and J. Tailleur, Passive objects in confined active fluids: A localization transition, Physical Review E **106**, 044604 (2022).
[38] M. Feng and Z. Hou, Unraveling on kinesin acceleration in intracellular environments: A theory for active bath, Physical Review Research **5**, 013206 (2023).
[39] A. Jayaram and T. Speck, Effective dynamics and fluctuations of a trapped probe moving in a fluid of active hard discs (a), Europhysics Letters **143**, 17005 (2023).
[40] R. Zakine, A. Solon, T. Gingrich, and F. Van Wijland, Stochastic stirling engine operating in contact with active baths, Entropy **19**, 193 (2017).

[41] E. W. Burkholder and J. F. Brady, Tracer diffusion in active suspensions, Physical Review E **95**, 052605 (2017).

[42] E. W. Burkholder and J. F. Brady, Fluctuation-dissipation in active matter, The Journal of Chemical Physics **150**, 10.1063/1.5081725 (2019).

[43] K. Kanazawa, T. G. Sano, A. Cairoli, and A. Baule, Loopy lévy flights enhance tracer diffusion in active suspensions, Nature **579**, 364 (2020).

[44] J. Reichert and T. Voigtmann, Tracer dynamics in crowded active-particle suspensions, Soft Matter **17**, 10492 (2021).

[45] L. Abbaspour and S. Klumpp, Enhanced diffusion of a tracer particle in a lattice model of a crowded active system, Physical Review E **103**, 052601 (2021).

[46] Z. Peng and J. F. Brady, Forced microrheology of active colloids, Journal of Rheology **66**, 955 (2022).

[47] I. Santra, Dynamical fluctuations of a tracer coupled to active and passive particles, Journal of Physics: Complexity **4**, 015013 (2023).

[48] T. Dhar and D. Saintillan, Active transport of a passive colloid in a bath of run-and-tumble particles, Scientific Reports **14**, 10.1038/s41598-024-62396-2 (2024).

[49] P. Dolai, A. S. Rajput, and K. V. Kumar, Shape-dependent motility of polar inclusions in active baths, Physical Review E **110**, 014607 (2024).

[50] Y. Zhao, R. Zakine, A. Daerr, Y. Kafri, J. Tailleur, and F. van Wijland, Active young-dupré equation: How self-organized currents stabilize partial wetting (2024), arXiv:2405.20651 [cond-mat.soft].

[51] R. Sarkar, I. Santra, and U. Basu, Harmonic chain driven by active rubin bath: transport properties and steady-state correlations, Proceedings of the Royal Society A: Mathematical, Physical and Engineering Sciences **480**, 10.1098/rspa.2024.0275 (2024).

[52] C. Maes, Fluctuating motion in an active environment, Physical Review Letters **125**, 208001 (2020).

[53] S. Steffenoni, K. Kroy, and G. Falasco, Interacting brownian dynamics in a nonequilibrium particle bath, Physical Review E **94**, 062139 (2016).

[54] O. Granek, Y. Kafri, and J. Tailleur, Anomalous transport of tracers in active baths, Physical Review Letters **129**, 038001 (2022).

[55] A. Solon and J. M. Horowitz, On the Einstein relation between mobility and diffusion coefficient in an active bath, Journal of Physics A: Mathematical and Theoretical **55**, 184002 (2022).

[56] J. Tailleur and M. E. Cates, Statistical mechanics of interacting run-and-tumble bacteria, Physical Review Letters **100**, 218103 (2008).

[57] P. Romanczuk, M. Bär, W. Ebeling, B. Lindner, and L. Schimansky-Geier, Active brownian particles: From individual to collective stochastic dynamics, The European Physical Journal Special Topics **202**, 1 (2012).

[58] A. P. Solon, M. E. Cates, and J. Tailleur, Active brownian particles and run-and-tumble particles: A comparative study, The European Physical Journal Special Topics **224**, 1231 (2015).

[59] K. Malakar, V. Jemseena, A. Kundu, K. Vijay Kumar, S. Sabhapandit, S. N. Majumdar, S. Redner, and A. Dhar, Steady state, relaxation and first-passage properties of a run-and-tumble particle in one-dimension, Journal of Statistical Mechanics: Theory and Experiment **2018**, 043215 (2018).

[60] U. Basu, S. N. Majumdar, A. Rosso, and G. Schehr, Active brownian motion in two dimensions, Physical Review E **98**, 062121 (2018).

[61] T. Demaerel and C. Maes, Active processes in one dimension, Physical Review E **97**, 032604 (2018).

[62] L. Caprini, A. R. Sprenger, H. Löwen, and R. Wittmann, The parental active model: A unifying stochastic description of self-propulsion, The Journal of Chemical Physics **156**, 10.1063/5.0084213 (2022).

[63] L. DAlessio, Y. Kafri, and A. Polkovnikov, Negative mass corrections in a dissipative stochastic environment, Journal of Statistical Mechanics: Theory and Experiment **2016**, 023105 (2016).

[64] T. Tanogami, Violation of the second fluctuation-dissipation relation and entropy production in nonequilibrium medium, Journal of Statistical Physics **187**, 10.1007/s10955-022-02921-7 (2022).

[65] J.-H. Pei and C. Maes, Induced friction on a probe moving in a nonequilibrium medium, Physical Review E **111**, l032101 (2025).

[66] T. Harada and S.-i. Sasa, Energy dissipation and violation of the fluctuation-response relation in nonequilibrium langevin systems, Physical Review E **73**, 026131 (2006).

[67] C. Maes, On the second fluctuationdissipation theorem for nonequilibrium baths, Journal of Statistical Physics **154**, 705 (2014).

[68] K.-W. Kim, Y. Choe, and Y. Baek, Symmetry-breaking motility of penetrable objects in active fluids, Physical Review E **109**, 014614 (2024).

[69] J.-H. Pei and C. Maes, Supplemental material (2025).

[70] M. Itami and S.-i. Sasa, Universal form of stochastic evolution for slow variables in equilibrium systems, Journal of Statistical Physics **167**, 46 (2017).

[71] U. Erdmann, W. Ebeling, L. Schimansky-Geier, and F. Schweitzer, Brownian particles far from equilibrium, The European Physical Journal B **15**, 105 (2000).

[72] A. Dhar, A. Kundu, S. N. Majumdar, S. Sabhapandit, and G. Schehr, Run-and-tumble particle in one-dimensional confining potentials: Steady-state, relaxation, and first-passage properties, Physical Review E **99**, 032132 (2019).

[73] M. V. Moreno, D. G. Barci, and Z. G. Arenas, State-dependent diffusion in a bistable potential: Conditional probabilities and escape rates, Physical Review E **101**, 062110 (2020).

[74] The Lennard-Jones force here uses a different set of parameters compared to its common form. k_0 is chosen to be $\frac{42}{169}\sqrt[6]{\frac{7}{13}}$. This choice benefits the comparison with 1D case. Here, R corresponds to zero-force distance, characterizing the size of the probe. k equals the maximum amplitude of the attraction and determines whether the medium particles are trapped by the probe.

END MATTER

Expressions of velocity-dependent friction and noise

In this section, we show the concrete expressions for $f(v)$, $B(v)$, and $G(v)$, respectively in 1D and 2D.

In 1D, quantities in Eq. (5) are given by

$$\begin{aligned} f(v) &= N \langle F(r) \rangle_v , \\ B(v) &= N \int_0^\infty \mathrm{d}s \, \langle F(r(s)); F(r(0)) \rangle_v , \\ G(v) &= N \int_0^\infty \mathrm{d}s \left\langle F(r(s)); F(r(0)) \frac{\partial}{\partial v} \log \rho_v(r(0)) \right\rangle_v . \end{aligned} \tag{15}$$

For fixed boundary length L, all three quantities are proportional to the number of medium particles N. Here, we introduce a fixed-v dynamics for a single variable r (relative position of medium particle), given by Eq. (4) with probe velocity v fixed. In the above formulas, $\rho_v(r)$ is the stationary distribution in the fixed-v dynamics, $\langle \ldots \rangle_v$ denotes the stationary average, and $\langle \star; \circ \rangle_v = \langle \star \circ \rangle_v - \langle \star \rangle_v \langle \circ \rangle_v$ denotes the connected correlation (covariance).

In 2D, quantities in Eq. (12) are given by

$$\begin{aligned} f(v) &= N \langle F_\parallel \rangle_{\mathbf{v}} \\ B_\parallel(v) &= N \int_0^\infty \mathrm{d}s \, \langle F_\parallel(r(s)); F_\parallel(r(0)) \rangle_{\mathbf{v}} , \\ B_\perp(v) &= N \int_0^\infty \mathrm{d}s \, \langle F_\perp(s); F_\perp(0) \rangle_{\mathbf{v}} , \\ G(v) &= N \int_0^\infty \mathrm{d}s \, \langle F_\parallel(r(s)); F_\parallel(r(0)) \partial_v \log \rho_{\mathbf{v}}(r(0)) \rangle_{\mathbf{v}} . \end{aligned} \tag{16}$$

$F_\parallel$ and $F_\perp$ represent the interaction force in the tangential and perpendicular directions with respect to the probe velocity, respectively. Similar to 1D, the fixed-$\mathbf{v}$ dynamics for the relative position $\mathbf{r}$ of a single medium particle is given by Eq. (11) with fixed probe velocity (v_x, v_y). In the above formula, $\langle \ldots \rangle_{\mathbf{v}}$ and $\rho_{\mathbf{v}}$ respectively denote the average and the stationary distribution in the fixed-$\mathbf{v}$ dynamics.

In both 1D and 2D, all quantities can be obtained from the analysis of the fixed-v/fixed-$\mathbf{v}$ dynamics, which is essentially a nonequilibrium dynamics for a single medium particle. They can be calculated or analyzed easily from either theoretic or numerical methods.

Intuitive analysis of nonlinear friction

Here, we provide a theoretical analysis of $f(v)$ in 1D and 2D.

We specify the setup of our analysis in 1D. We consider that a repulsive interaction with a maximum force $F_{\max} = \max_r F(r)$ and an interaction range R. Hardcore interaction refers to the case of $F_{\max} = \infty$, while soft interaction means that $F_{\max}$ is finite. The expression of $f(v)$ in (15) involves an average in the fixed-v dynamics. In the following, we assume the probe is moving at fixed velocity $v \geq 0$ (from left to right) to analyze that average, noting that $f(v)$ is antisymmetric, $f(-v) = -f(v)$.

We first consider the large persistence limit of the medium $\alpha R/u \to 0$, where we can assume that half of medium particles have fixed $\sigma = +1$ while the others have fixed $\sigma = -1$.

(0) For hardcore interactions: friction is purely positive. Medium particles with certain σ get stuck at the same distance, as is shown in Fig. 3(a). Each medium particle with $\sigma = +1$ pushes the probe with force $\mu(u-v)$, while particle with $\sigma = -1$ exerts a force $-\mu(u+v)$. The total force (15) on the probe becomes $-f(v) = -N\mu v$, indicating a positive and linear friction.

For soft interaction, we further distinguish several cases according to the magnitude of $F_{\max}$.

(1) Small interaction amplitude $F_{\max} < \mu u$: the sign structure of $f(v)$ is $(-,+)$, corresponding to the peculiar regime (R2a).

For small probe velocity $0 \leq v < u - F_{\max}/\mu$, the medium particles are able to pass through the probe. We consider medium particles with $\sigma = +1$ (moving in the same direction as the probe) and $\sigma = -1$ (moving in the opposite direction) separately, noticing that the medium stationary distribution is inversely proportional to the relative velocity $|\dot{r}|$. For medium particles with $\sigma = +1$, $|\dot{r}| = u - v + F(r)/\mu$ is smaller behind the probe ($r < 0$), resulting in higher density there (Fig. 3b). For medium particles with $\sigma = +1$, $|\dot{r}| = u - v + F(r)/\mu$ is smaller in front of the probe ($r > 0$), resulting in higher density there (Fig. 3c). The density asymmetry for $\sigma = +1$ dominates, causing a higher medium density behind the probe than in front of the probe. This density difference pushes the probe in the direction of its motion, resulting in negative friction.

The above analysis is for small probe velocity. For large enough v, medium particles with $\sigma = +1$ cannot catch up with the probe, leading to $f(v) > 0$ for large v.

(2) $F_{\max} \gtrsim \mu u$ (maximum repulsion is a bit larger than propulsion force): the sign structure of $f(v)$ is $(+,-,+)$, corresponding to the peculiar regime (R2b).

The medium particles get stuck for small v, as shown in Fig. 3(d). Similar to the hardcore case, the overall $f(v)$ is positive, linearly increasing with respect to v.

Nevertheless, for larger v such that $v + u > F_{\max}/\mu$ (but still $v < u$), medium particles with $\sigma = -1$ are able to pass through the probe while particles with $\sigma = +1$ are still stuck; see Fig. 3(e). Medium particles with $\sigma = -1$ still have a positive contribution to $f(v)$ but much less than that when they are stuck. Therefore, $f(v)$ can decrease to a negative value. At the threshold velocity $v + u = F_{\max}/\mu$, there is a singularity in the stationary distribution ρ_v, and $f(v)$ drops suddenly, which accounts for the singular turn over in Fig. 1(b).

For very large v such that $v > u$, $f(v)$ becomes positive again.

(3) $F_{\max} \gg \mu u$: the interaction is very large and effectively hardcore. $f(v)$ is purely positive.

For large flip rate α (small persistence), run-and-

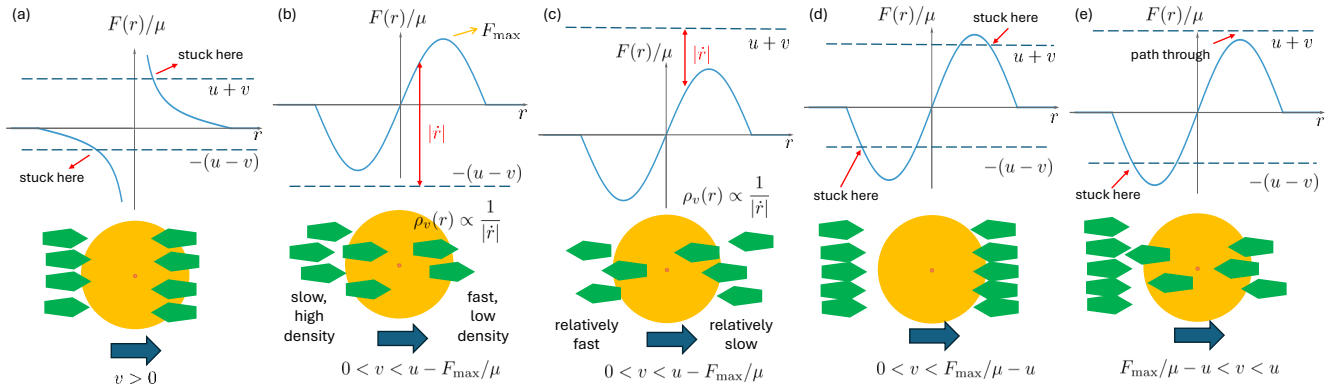


FIG. 3. Mechanism in 1D: The green pentagon represents the medium particles, the acute angles of which denote their propulsion direction. The yellow disk represents the probe, moving rightwards. The blue solid line represents the force (divided by μ) exerted on the medium particles. If medium particles can pass through the probe, the distance (shown in red) between $F(r)/\mu$ and $u+v$ or $-(u-v)$ yields the relative velocity $|\dot{r}|$ at different position r.

tumble motion resembles (passive) Brownian motion with diffusivity $D = u^2/(2\alpha)$ [58], and the medium reduces to an equilibrium medium. For an equilibrium medium, we know that the friction $f(v)$ is always positive.

In summary, for either (effectively) hardcore interaction or large α, the behavior of $f(v)$ belongs to the passive regime (R1). For soft interaction and small α, if $F_{\max} < \mu u$, $f(v)$ behaves as in the active regime (R2a), and if $F_{\max} \gtrsim \mu u$, we get the active regime (R2b).

For 2D, the mechanism is much more complicated than that in 1D. Medium particles can pass by a hardcore probe. We discuss how the negative friction can appear for an interaction with a hardcore.

We focus on the case of high-persistence limit, $\alpha R/u \to 0$. In this intuitive analysis, we roughly divide a hardcore interaction into two parts: a core region and a peripheral region. In the core region, the repulsive force between the probe and medium particles is large, so that medium particles hardly enter this region. The peripheral region is outside the core region, where the interaction force is smaller than but comparable to the propulsion force, either repulsive or attractive. Medium particles can enter and depart this region easily.

When a bath particle interacts with the probe, there are two cases. In the first case, the bath particle hits the core region and feels a strong repulsion. It then slows down and moves along the boundary of core region before leaving. This kind of events is similar to the 1D case where bath particles are stuck, resulting in a positive contribution to the friction. In the second case, the bath particle enters the peripheral region but does not hit the core region. Since the interaction is not large, the trajectory of the particle only deviates slightly from a straight line during the interaction. This kind of events is similar to the 1D case where bath particles pass through the probe. It results in a negative friction, pushing the probe in the same direction as its motion.

The total friction is a competition of the two contributions. In order for negative friction, most bath particles should pass through the peripheral region rather than collide with the core region. Therefore, the interaction should have a large peripheral region and a small core region. This means that the interaction decays slowly as the distance increases instead of being direct collision. In addition, an interaction with attraction at large distance (such as Lennard-Jones) is preferable than a purely repulsive one. The attractive part captures a lot of bath particles in the peripheral region, enhancing the negative contribution.

In SM [69], we provide a set of plots, showing how different interaction strengths of the Lennard-Jones force, by altering the two contributions, lead to different regimes of probe motion in 2D.